# Effects of Pump Power in Doppler-free Saturation Spectroscopy of Rubidium

Lukas Kostal

***Abstract*—The theory of hyperfine atomic structure and the interaction of a 2 level atom with EM radiation are introduced and used to derive expressions for the amplitude and FWHM of a resonance peak as a function of the incident EM radiation intensity. The principles of Doppler-free saturated absorption spectroscopy are explained. An experiment for Doppler-free spectroscopy of the Rubidium $D_2$ line featuring a Fabry-Pérot etalon for frequency calibration is described. Measurements for a range of pump powers are taken to obtain curves of peak amplitude and FWHM against the total incident power.**

**The frequency differences between the transitions caused by the hyperfine splitting of the final state $5^2P_{3/2}$ are shown to agree with theoretical values to within the expected uncertainty. The observed dependance of the peak amplitude on the total incident power is shown to agree with the theoretical model with a reduced chi-squared value of $\chi^2_\nu = 0.633$ (3sf) giving a saturation power of $P_{\text{sat}} = 610 \pm 180$ $\mu$W. Power broadening is clearly observed and shown to agree with the theoretical model with a reduced chi-squared value of $\chi^2_\nu = 0.0878$ (3sf) giving a saturation power of $P_{\text{sat}} = 590 \pm 180$ $\mu$W. The natural linewidth is determined to be $\Gamma = 8.18 \pm 0.51$ MHz which does not agree with the theoretical value of $\Gamma = 5.746(8)$ MHz to within the expected uncertainty.**

**Potential sources of this discrepancy are discussed and it is argued to be caused by transit time broadening and the recoil effect. Finally, future improvements of the experimental setup are presented and further investigation is discussed.**

## I. Introduction

Spectroscopy provides a method for studying properties of quantum systems such as atoms and molecules via their interaction with electromagnetic (EM) radiation. In practice the resolution of the obtained spectra is limited by Doppler broadening caused by the thermal motion of atoms and molecules.

Following the invention of narrow band laser sources, a new spectroscopy technique called Doppler-free saturated absorption spectroscopy was introduced to eliminate the effects of Doppler broadening without the need for cooling the sample down to cryogenic temperatures. The technique is commonly featured in frequency locking schemes where a feedback loop is used to maintain the frequency of a laser in resonance with a specific transition. Frequency locked lasers have a wide range of applications in research for example in laser cooling of atoms and molecules, interferometry in high precision low energy physics or in atomic clocks.

The resolution of Doppler-free spectra is still limited by the remaining physical effects giving rise to broadening. Of these the most significant is power broadening caused by the power of the incident EM radiation [1]. It is therefore desirable to study the effects of pump power on hyperfine transition peaks in order to be able to optimise the pump power based on the requirements of a particular Doppler-free saturation spectroscopy application.

## II. Theory

### A. Rubidium Atom

Rubidium is an alkali metal with a single valence electron and an electron configuration $[\text{Kr}]\,5\text{s}^1$. The 2 naturally occurring isotopes of Rubidium are $^{85}$Rb and $^{87}$Rb with relative abundances $72.17\%$ and $27.83\%$ respectively [2]. Due to the different number of neutrons the isotopes have total nuclear spin quantum numbers $I = 5/2$ and $I = 3/2$ for $^{85}$Rb and $^{87}$Rb respectively.

The measured hyperfine transitions correspond to the Rb $\text{D}_2$ line with a wavelength of $\lambda = 780.24$ nm in the near-infrared (NIR) part of the spectrum. The initial state $5^2\text{S}_{1/2}$ has quantum numbers $l = 0, s = 1/2, j = 1/2$ and is split into 2 hyperfine levels with quantum numbers $f = 2, 3$ and $f = 1, 2$ for $^{85}$Rb and $^{87}$Rb respectively. The final state $5^2\text{P}_{3/2}$ has quantum numbers $l = 1, s = 1/2, j = 3/2$ and is split into 4 hyperfine levels $f' = 1, 2, 3, 4$ for $^{85}$Rb and $f' = 0, 1, 2, 3$ for $^{87}$Rb.

A selection rule requires the change in the $f$ quantum number to be $\Delta f = -1, 0, +1$ giving 3 possible transitions for each initial state. This results in a total of 12 hyperfine transition peaks with 6 distinct frequency differences $\Delta\nu$ which characterise the hyperfine splitting of the $5^2\text{P}_{3/2}$ state.

### B. Hyperfine Structure

The hyperfine structure is a result of the interaction of the magnetic dipole moment corresponding to the total angular momentum of the electron and the spin angular momentum of the nucleus with operators $\hat{\boldsymbol{J}}$ and $\hat{\boldsymbol{I}}$ respectively. This interaction is accounted for by introducing the total angular momentum of the atom with an operator $\hat{\boldsymbol{F}} = \hat{\boldsymbol{J}} + \hat{\boldsymbol{I}}$ and a quantum number $f = j + I$.

A Hamiltonian for the interaction can be written as

$$\hat{H}_{\text{hfs}} = -\hat{\boldsymbol{\mu}}_I \cdot \vec{B}_J \tag{1}$$

$$= A_{\text{hfs}} \hat{\boldsymbol{I}} \cdot \hat{\boldsymbol{J}} \tag{2}$$

Where $\hat{\boldsymbol{\mu}}_I$ is the operator corresponding to the magnetic dipole moment of the nucleus and $\vec{B}_J$ is the magnetic field due to the total angular momentum of the electron at the position of the nucleus. The magnetic dipole constant $A_{\text{hfs}}$ is introduced to account for the geometry of the magnetic dipole interaction.

Additionally, the hyperfine structure also includes an electric quadrupole moment and magnetic octupole moment interactions with constants $B_{\text{hfs}}$ and $C_{\text{hfs}}$ as described in [3].

Using time-independent perturbation theory, the 1st order hyperfine correction to the energy of a state characterised by quantum numbers $n, l, j, f, m_f$ is given by (4) [4].

$$\delta E^{(1)}_{\text{hfs}} = \langle n,l,j,f,m_f|\hat{H}_{\text{hfs}}|n,l,j,f,m_f\rangle \tag{3}$$
$$= \langle A_{\text{hfs}}\rangle \left(f\left(f+1\right) - j\left(j+1\right) - I\left(I+1\right)\right) \tag{4}$$

From Eq. (4) the energy difference between 2 hyperfine levels $f_1$ and $f_2$ can be calculated as

$$\Delta E_{\text{hfs}}(f_1,f_2) = |\delta E^{(1)}_{\text{hfs}}\left(f_2\right) - \delta E^{(1)}_{\text{hfs}}\left(f_1\right)| \tag{5}$$

Which corresponds to a frequency difference given by

$$\Delta\nu(f_1,f_2) = \frac{\Delta E_{\text{hfs}}(f_1,f_2)}{h} \tag{6}$$

### C. Lorentz Model and Population Dynamics

The atom interacts with the electric field of an incident EM wave with an amplitude $\vec{\mathcal{E}_0}$ via an electric dipole moment of the atom with a corresponding operator $\hat{\boldsymbol{d}}$. The interaction can be modelled as a damped harmonic oscillator driven by the electric field. The absorption cross section $\sigma$ therefore has the form of a Lorentzian given by

$$\sigma(\nu) = \frac{\sigma_0\Gamma}{4(\nu-\nu_0)^2+\Gamma^2} \tag{7}$$

Where $\sigma_0$ is the absorption cross section at resonance related to the Einstein B coefficient, $\nu_0$ is the resonant frequency of the atom and $\Gamma$ is the FWHM of the Lorentzian response.

Treating the Rb atom as a simple 2 level system, the number of atoms in the initial state $N$ and the excited state $N'$ are described by a set of rate equations [5] shown below

$$\frac{dN}{dt} = \Gamma N' - g(\nu)\phi(N-N') \tag{8}$$

$$\frac{dN'}{dt} = -\Gamma N' + g(\nu)\phi(N-N') \tag{9}$$

Where $\Gamma$ is the Einstein coefficient corresponding to a spontaneous decay rate given by the reciprocal of the lifetime of the excited state $\Gamma = 1/\tau$. The rate of stimulated absorption and emission is given by $\sigma(\nu)\phi$ where $\phi$ is the photon flux of the incident EM radiation at frequency $\nu$.

A steady state solution of the rate equations is obtained in the limit as $t \to \infty$ in which the fraction of the atoms in the excited state is given by

$$\frac{N'}{N+N'} = \frac{1}{2}\frac{s\Gamma^2}{4(\nu-\nu_0)^2+(s+1)\Gamma^2} \tag{10}$$

A saturation parameter $s$ is defined as the ratio

$$s = \frac{\phi}{\phi_{\text{sat}}} = \frac{I}{I_{\text{sat}}} \tag{11}$$

Where $\phi_{\text{sat}}$ and $I_{\text{sat}}$ are the saturation incident photon flux and intensity at which $N' = N/4$. Saturation occurs in the limit as $s \to \infty$ and the steady state population is $N' = N$.

At resonance $\nu = \nu_0$ and Eq. (10) gives an expression for the amplitude $A_0$ of the hyperfine transition peak as

$$A_0 \propto \frac{s}{2(s+1)} \tag{12}$$

Similarly the FWHM $\Gamma$ of the power broadened hyperfine transition peak is given by

$$\Delta = \Gamma\sqrt{1+s} \tag{13}$$

Equations (12) and (13) describe how increasing the incident power results in an increase of the peak amplitude $A_0$ as well as the peak FWHM $\Delta$ giving rise to power broadening. This results in a tradeoff between the signal to noise (SNR) ratio of the measured signal and the the frequency resolution of the transition peak limited by power broadening.

## III. Principle of Operation

### A. Doppler-free Saturated Absorption Spectroscopy

Atoms at a non-zero temperature $T$ will have a root mean square (RMS) speed calculated as

$$v_{\text{rms}} = \sqrt{\frac{3k_BT}{m}} \tag{14}$$

Where $m$ is the mass of the atom and $k_B$ the Boltzmann constant. For Rb atoms at room temperature the RMS speed $v_{\text{rms}} = 292\ \text{ms}^{-1}$.

An atom moving with a velocity $\vec{v}$ with respect to an incident laser beam of frequency $\nu$ propagating with a wave vector $veck$ will see a Doppler shifted frequency $\nu'$ given by

$$\nu' = \nu\left(1+\frac{\vec{v}\cdot\vec{k}}{nc}\right) \tag{15}$$

Where $n$ is the the refractive index of the medium through which the beam propagates and $c$ is the speed of light in vacuum. By symmetry the component of $\vec{v}$ parallel to the laser beam will follow a Gaussian distribution.

In Doppler-free saturated absorption spectroscopy, two overlapping counter propagating beams are sent through the atomic vapour sample [6]. A higher power pump beam excites all atoms with velocities $\vec{v}\cdot\vec{k} = v_-$ such that they are in resonance with the Doppler shifted frequency $\nu_-$. A lower power probe beam propagating in the opposite direction also excites all atoms with velocities $\vec{v}\cdot\vec{k} = v_+$ such that they are in resonance with the Doppler shifted frequency $\nu_+$. This results in an overall Doppler-broadened absorption profile.

Atoms with a zero velocity component along the two beams $\vec{v}\cdot\vec{k} = 0$ will be in resonance with both the pump and the probe beam. As a result they are excited by the pump beam and de-excited by the probe beam by stimulated emission of a photon in the direction of the probe beam. This results in an increase of the measured probe beam intensity and therefore a narrow Doppler-free dip in the Doppler-broadened absorption profile.

For atoms with multiple hyperfine states giving transitions with resonant frequencies $\nu_1$ and $\nu_2$ where $|\nu_2-\nu_1| \sim \Gamma$, an additional crossover peak will be observed at exactly the average frequency $\nu = (\nu_2+\nu_1)/2$. This corresponds to atoms with velocities such that the pump beam is in resonance with one of the transitions and the probe beam with the other.

### B. Fabry-Pérot Etalon

A confocal Fabry-Pérot etalon (FPE) is an optical cavity composed of two plano-concave partially reflective surfaces separated by a distance $l$ equal to twice the focal length of the mirrors. Inside the cavity the incident light is reflected back and forth and interferes with itself. At resonance the cavity supports a transverse EM mode which results in partial transmission of the incident light giving Lorentzian peaks in the transmission spectrum of the FPE which can be used for frequency calibration.

The frequency difference between consecutive peaks is given by the free spectral range (FSR). In a confocal FPE all higher order modes are degenerate and therefore contribute to a single peak in between peaks corresponding to 1st order modes. As a result the FSR is given by

$$\text{FSR} = \frac{nc}{4l} \tag{16}$$

Where $nc$ is the speed of light inside the FPE of length $l$ [7].

The FPE used in the experimental setup is observed to support a total of $8$ modes all of which appear to be non-degenerate resulting in $8$ distinct peaks. To account for this the FSR is taken to be

$$\text{FSR} = \frac{nc}{18l} \tag{17}$$

The FWHM of the Lorentzian FPE transmission peaks is limited by the round trip losses in the resonant cavity affected by factors such as the quality of mirrors and alignment. The FWHM is related to a finesse parameter $\mathcal{F}$ as

$$\mathcal{F} = \frac{\text{FSR}}{\Gamma} \tag{18}$$

Where $\Gamma$ is the FWHM of the Lorentzian transmission peak.

## IV. Experimental Setup

The experimental setup is constructed on a vibrationally isolated optical table as shown in Fig. 1.

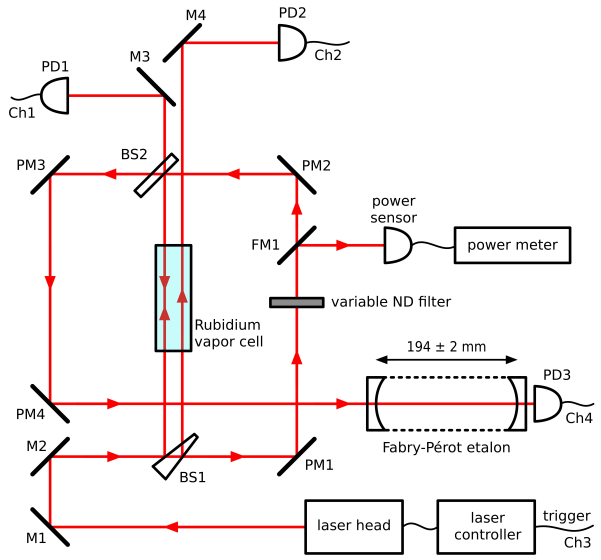


Fig. 1: Schematic of the optical setup for Doppler-free saturated absorbtion spectroscopy using a tunable diode laser and a Fabry-Pérot etalon.

The laser source used is a Toptica DL pro 780 tunable external cavity diode laser controlled by a Toptica DLC pro digital laser controller. The laser features a Littrow configuration external cavity with a reflective diffraction grating mounted on a piezoelectric stack which allows for the length of the resonant cavity to be adjusted by applying a voltage across the piezo [8], [9]. This allows for mode-hop free tuning of the wavelength $\lambda$ of the laser. The controller is set to apply a triangular waveform to the piezo scanning the wavelength over the range of the hyperfine transitions in the Rb $D_2$ line.

The Rb sample used is a Thorlabs GC25075-RB Rubidium vapour reference cell.

The power of the probe beam, pump beam and the transmission of the FPE are measured using the Thorlabs PDA36A-EC Si photodiode detectors featuring a transimpedance amplifier with variable gain. The detectors are connected to a Rhode & Schwartz RTB2004 digital storage oscilloscope as shown in Fig. 1 with an external trigger signal on Ch3 from the laser controller.

Mirrors labelled PM1 to PM4 are mounted in kinematic mounts with piezoelectric inertial actuators to allow for safe remote alignment with the NIR laser beam on.

The power of the pump beam is adjusted using a continuously variable neutral density (ND) filter mounted in between PM1 and PM2. The power behind the ND filter is measured using the Thorlabs S130C photodiode power sensor connected to the P400 power meter unit. A flip mirror FM1 is mounted behind the ND filter and used to reflect the beam onto the power sensor during power measurements.

## V. Methodology

First an alignment of the pump and probe beam is performed by observing the Doppler-free signal on Ch1 and adjusting the orientation of mirrors PM1 and PM2 until the greatest amplitude of the Doppler free dips is observed.

To achieve resonance in the FPE the incident beam must be centred and collinear with the resonance cavity. An initial alignment is performed by measuring the position of a low power red alignment laser using a ruler and manually adjusting the orientation of mirrors PM3 and PM4. The NIR laser is then turned on and the length of the FPE cavity $l$ is adjusted by screwing the lens tube in which the front mirror is mounted. The length is adjusted until the peak observed on Ch4 are symmetric and the length is recorded to be $l = 194 \pm 2$ mm. Finally, a fine adjustment of PM3 and PM4 is performed using the piezoelectric actuators until the greatest possible height of the resonance peaks is achieved. The final finesse of the FPE is calculated to be $\mathcal{F} = 7.4 \pm 0.2$.

With the ND filter set to an optical density of OD $= 0$ the power of the probe and pump beams is measured at the surface of the Rb cell and recorded. The power of the probe beam is measured to be $P_{\text{probe}} = 8.5 \pm 0.3$ $\mu$W.

The gain of the photodiode detectors is set to the highest possible setting without saturating the built in amplifier. The horizontal scale on the oscilloscope is set to capture a sequence of at least 10 scans for averaging in data analysis. The built in 5 kHz lowpass filter is enabled and the acquisition memory depth is set to 5 MSa.

To begin a measurement the mirror FP1 is flipped to measure the power and the ND filter is adjusted to set the desired power which is then recorded. A set of 3 datasets is taken for each measurement. The input of the FPE is blocked to prevent back reflections throughout the system and a Doppler-free spectrum (DFS) dataset is saved. Next the probe beam is blocked using the flip mirror and a Doppler-broadened spectrum (DBS) dataset is saved. Finally, both the pump beam and the FPE are unblocked, the ND filter is set to OD $= 0$ and a dataset for the FPE transmission is saved.

The measurement process is then repeated to obtain a set of 14 measurements with the measured power varying from $500 \pm 15$ $\mu$W down to $2.0 \pm 0.1$ $\mu$W with increments adjusted such that an appropriate number of measurements is obtained across the entire saturation curve.

## VI. Analysis

The analysis is performed using a Python script which can be found in the GitHub Repository [10] of the experiment along with all of the collected datasets and additional results.

### A. Doppler-free Spectrum

For the analysis of a measurement at a given pump power all 3 datasets (DFS, DBS, FPE) are loaded. The waveforms are then sliced to correspond to individual scans based on the rising/falling edges in the trigger signal from the laser controller. The displacement of the piezoelectric stack responsible for the mode-hop free tuning of the laser is non-liner with respect to the applied voltage and exhibits hysteresis. It is decided to only consider waveforms for which the piezo is moving in the forward direction as this motion is more linear than in the reverse direction. The waveforms are then averaged to reduce the effects of random noise.

The doppler-free absorption signal is obtained by subtracting the Ch1 waveform in the DFS dataset from the Doppler-broadened waveform in the DBS dataset. The resulting Doppler-free spectrum is then normalised and the normalisation constant $A_{\text{norm}}$ is saved for further analysis. The expected uncertainty on the normalised absorbance is taken to be the peak-to-peak value of the background noise.

### B. Frequency Calibration

The FPE data is used to obtain a calibration curve for mapping the scan time $t$ into a relative frequency of the laser $\nu$. The FPE signal is normalised and an algorithm is used to detect the position of the resonance peaks and estimate their FWHM $\Gamma$. Next a Lorentzian function is fitted on an interval of width $2\Gamma$ centred around each peak. The scan time at the center of the peak $t_0$ and the FWHM $\Gamma$ is obtained from the optimised parameters with expected uncertainties calculated from the covariance matrix. The mean FWHM is used to calculate the finesse $\mathcal{F}$ of the FPE. The frequency of each peak is calculated as the order of the peak times the FSR and is plotted against the scan time $t_0$ at which each peak occurs. Since the FSR is much smaller than the absolute frequency of the laser light FSR $\ll \lambda/c$, in between the FPE peaks the frequency can be approximated as varying linearly with the wavelength and therefore the scan time $t$. This justifies the use of linear interpolation to obtain a calibration curve of relative frequency $\nu$ against the scan time $t$. The expected uncertainty in frequency is calculated by propagating the uncertainty in the length of the FPE cavity $l$ and the time $t_0$ from the optimised parameters through the linear interpolation.

### C. Resonance Frequencies

The spectrum measured at is then sliced into 4 sections corresponding to the 2 different initial states of the 2 isotopes of Rb. An algorithm is used to find the position and approximate power broadened FWHM $\Delta$ of the hyperfine transition and crossover peaks. Approximating the baseline around the peaks as linear, a Lorentzian with a linear baseline is fitted on an interval $2\Delta$ centred around each of the peaks. The relative resonant frequency $\nu_0$ and power broadened FWHM $\Delta$ are determined from the optimised parameters with expected uncertainties calculated from the covariance matrix.

The use of asymmetric least square (ALS) smoothing to remove the baseline from the spectrum [11] was also tested instead of approximating the baseline as linear. In the end it was decided not to use ALS smoothing as there is no statistically rigorous method for optimising the ALS parameters. Furthermore, it was found that applying ALS smoothing resulted in slight shifts of the obtained relative resonant frequencies $\nu_0$ and an inferior Lorentzian fit.

Frequency differences $\Delta\nu$ are then calculated from the relative resonant frequencies $\nu_0$ measured at a pump power of $55.6 \pm 2.9$ $\mu$W. Furthermore, the position of the crossover peaks can be used to improve the accuracy of the detuning frequencies since they lie exactly in between two hyperfine transition peaks.

### D. Effects of Pump Power

To investigate the effects of varying the power of the pump beam the peak corresponding to the $^{87}$Rb transition $5^2\text{S}_{1/2}\ f = 2 \rightarrow 5^2\text{P}_{3/2}\ f' = 3$ is chosen due to its relatively high amplitude, low baseline and isolation from other peaks.

The power of the pump beam is calculated by scaling the power measured by the ND filter to account for the fraction of the power reflected by the beam splitter BS2 into the Rb cell. The total incident power on the Rb cell $p_{\text{tot}}$ is then found by adding the measured power of the probe beam.

The amplitude of the chosen peak is first corrected for the normalisation factor $A_{\text{norm}}$ giving a corrected amplitude $A_0$. A saturation curve is then obtained by plotting the corrected amplitude against the total incident power. The theoretical expression given by Eq. (12) is fitted onto the data using orthogonal distance regression [12] which accounts for uncertainties on both the dependant and independent variables. The saturation power $P_{\text{sat}}$ is determined from the optimised parameters and an RCS test is performed.

A power broadening curve is obtained by plotting the FWHM $\Delta$ of the power broadened peak against the total incident power. The theoretical expression for power broadening given by Eq. (13) is fitted onto the data using orthogonal distance regression. The natural linewidth FWHM $\Gamma$ as well as saturation power $P_{\text{sat}}$ are obtained from the optimised parameters with uncertainties calculated from the covariance matrix and a reduced chi-squared test is performed.

## VII. Results and Discussion

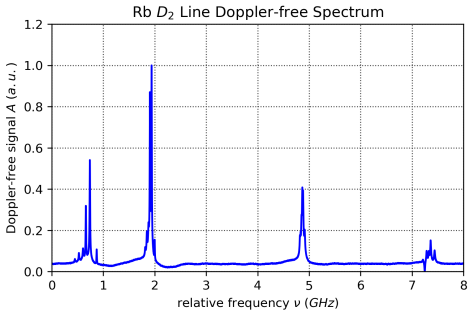


Fig. 2: Plot of the entire Doppler-free absorption spectrum of the Rb $D_2$ line with labels corresponding to different initial hyperfine states.

On Fig. 2 it can be seen that the hyperfine splitting of the initial state $5^2S_{1/2}$ is on the order of 1 GHz which is significantly greater than the hyperfine splitting of the excited state $5^2P_{3/2}$ with orders of only up to 100 MHz. This is because in the initial state $5^2S_{1/2}$ the probability density function of the electron's position has a higher amplitude in regions closer to the nucleus. As a result the coupling between the total electron angular momentum and nuclear spin angular momentum is greater resulting in a higher energy difference between the hyperfine states.

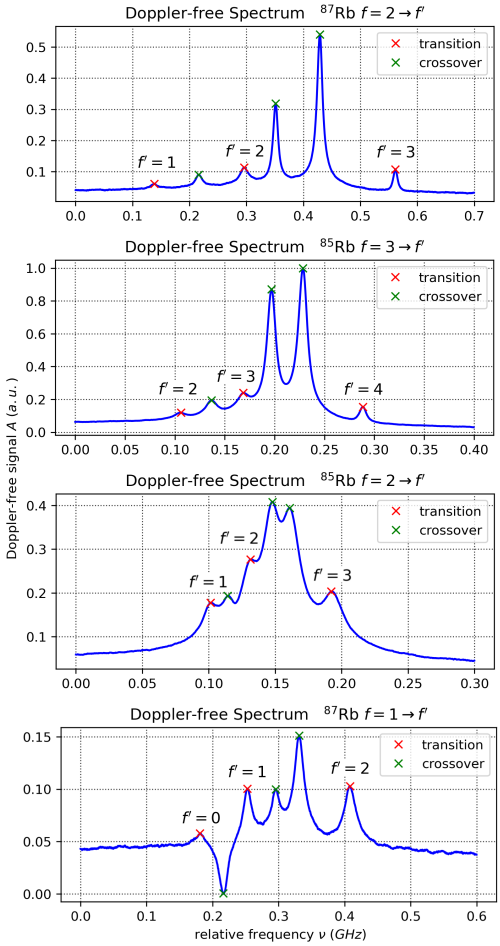


Fig. 3: Plots of sets of peaks corresponding to a specific initial level with labels corresponding to different final hyperfine states.

On Fig. 3 it can be seen that there are 3 peaks labelled in red corresponding to the 3 hyperfine states of $5^2P_{3/2}$ the transition to which follows the selection rule $\Delta f = -1, 0, +1$. Furthermore there are 3 crossover peaks labelled in green which lie exactly in between the corresponding hyperfine transitions peaks as previously discussed. The amplitude of the crossover peaks is observed to be greater than the amplitude of the hyperfine transition peaks. This is because the crossover peaks in this case are a result of resonance between 1 initial state and 2 final states which form a 3 levels system for which the amplitude at resonance is greater.

The first crossover resonance on the $^{87}$Rb $f = 1 \to f'$ spectrum can be observed to give rise to a dip as opposed to a peak. This is a result of an increased absorption and musts therefore correspond to a resonance regime of the 3 level system with final states $f' = 0, 1$ in which no significant stimulated emission occurs.

TABLE I: Measured and theoretical values for frequency difference in hyperfine levels of $5^2P_{3/2}$. Theoretical values obtained from [3] [13].

| isotope | transitions | $\Delta\nu_{\text{mes}}$ (MHz) | $\Delta\nu_{\text{the}}$ (MHz) |
|---|---|---|---|
| $^{87}$Rb | $f = 2 \to f' = 1, 2$ | $158.0 \pm 2.5$ | 156.947(7) |
| $^{87}$Rb | $f = 2 \to f' = 2, 3$ | $265.8 \pm 1.3$ | 266.650(9) |
| $^{85}$Rb | $f = 3 \to f' = 2, 3$ | $63.5 \pm 1.4$ | 63.401(61) |
| $^{85}$Rb | $f = 3 \to f' = 3, 4$ | $120.32 \pm 0.70$ | 120.640(68) |
| $^{85}$Rb | $f = 2 \to f' = 1, 2$ | $29.45 \pm 0.83$ | 29.372(9) |
| $^{85}$Rb | $f = 2 \to f' = 2, 3$ | $63.4 \pm 1.0$ | 63.401(61) |
| $^{87}$Rb | $f = 1 \to f' = 0, 1$ | $70.6 \pm 2.5$ | 72.218(4) |
| $^{87}$Rb | $f = 1 \to f' = 1, 2$ | $155.57 \pm 0.75$ | 156.947(7) |

The results in Tab. I show that all of the measured frequency differences $\nu$ between the hyperfine levels of the final state $5^2P_{3/2}$ agree with the theoretical values [3], [13] to within the expected uncertainty with a mean percentage deviation of $0.600 \pm 0.084\%$. There is no constant shift between the measured and theoretical values and so it can be concluded that there is no systematic error in the frequency calibration.

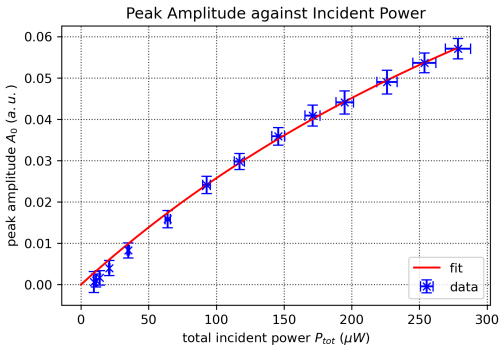


Fig. 4: Plot showing the effect of the total incident power on the amplitude of the $^{87}$Rb $f = 2 \to f' = 3$ hyperfine transition peak.

As shown in Fig. 4 increasing the total incident power results in an increase of the amplitude $A_0$ of the hyperfine transition peaks. The theoretical expression given by Eq. (12) fits the data with an RCS value of $\chi^2_\nu = 0.633$ (3sf) from which it can be concluded that the theoretical model agrees with the obtained data. The saturation power determined from the optimised parameters is $P_{\text{sat}} = 610 \pm 180$ $\mu$W corresponding to a percentage uncertainty of 29.5% (3sf).

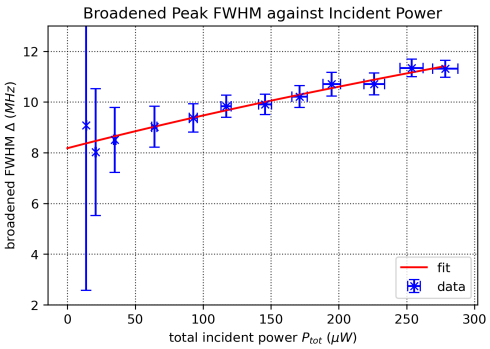


Fig. 5: Plot showing the effect of the total incident power on the FWHM of the $^{87}$Rb $f = 2 \rightarrow f' = 3$ hyperfine transition peak.

The effects of power broadening are clearly visible on Fig. 5 with the FWHM $\Delta$ increasing as the power of the pump beam is increased. The theoretical expression given by Eq. (13) fits the data with an RCS value of $\chi^2_\nu = 0.0878$ (3sf). The saturation power determined from the optimised parameters is $P_{\text{sat}} = 590 \pm 180$ $\mu$W which agrees with the value obtained from the peak amplitude curve to within the expected uncertainty with a percentage deviation of $3.33\%$ (3sf).

As the total incident power decreases the amplitude of the hyperfine peaks $A_0$ and therefore the signal to noise ratio decreases resulting in a greater uncertainty on the FWHM $\Delta$ from the Lorentzian fit. This causes the increasing size of the error bars in Fig. 5 as the total incident power decreases. The FWHM from the 3 lowest power measurements are not included since the amplitude of the peaks is comparable to the amplitude of the background noise.

The natural linewidth FWHM $\Gamma$ is determined to be $\Gamma = 8.18 \pm 0.51$ MHz. The theoretical value of the natural linewidth is $\Gamma = 5.746(8)$ MHz [13] so the measured value does not agree with the theoretical value to within the expected uncertainty. Since the measured value is greater than the theoretical value the discrepancy must be caused by broadening processes other than power broadening.

The pressure broadening coefficient for the Rb $D_2$ line has a value of $21.2$ MHzTorr$^{-1}$ [14]. The vapour pressure of the Rb inside of the cell is on the order of no more than $10^{-6}$ Torr and so the high measured linewidth can not be caused by pressure broadening.

Splitting caused by the Zeeman effect in the presence of a weak magnetic field can also give rise to broadening of the linewidth. The Zeeman shift coefficient of the Rb $D_2$ line is $575.15$ HzG$^{-2}$. The discrepancy of $2.43 \pm 0.51$ MHz would therefore correspond to a magnetic flux density on the order of $10$ G whereas the magnetic flux density at the surface of the Earth is only in the range of $0.25 - 0.65$ G

The leading cause of the discrepancy in the value of $\Gamma$ is therefore the transit time broadening [15]. This occurs because atoms in resonance with both the probe and pump beams have a zero velocity component along the two beams but are still free to move perpendicular to the beams. In the case of a narrow beam with a non-uniform beam profile the amplitude of the EM radiation experienced by the atom changes as it moves across the beam giving rise to transition time broadening.

Another significant cause of broadening in the experiment is the recoil effect. The recoil effect is a result of the conservation of linear momentum during emission and absorption of EM radiation by the atoms [16], [17].

## VIII. Conclusion

The theory of hyperfine atomic structure has been introduced giving the expression for the frequency difference between 2 hyperfine energy levels given by Eq. (6). A model of the interaction of a 2 level atom with EM radiation has been used to derive Eq. (12) and (13) which describe the effects of incident intensity on the amplitude and FWHM of hyperfine transition peaks. An experimental setup for Doppler-free spectroscopy of Rb utilising a FPE for frequency calibration was described and an analysis performed to obtain curves of peak amplitude and FWHM $\Delta$ against the total incident power.

The frequency differences between the transition peaks are shown to agree with the theoretical values to within the expected uncertainty with a mean percentage deviation of $0.600 \pm 0.084\%$. The expression for the transition peak amplitude given by Eq. (12) is shown to fit the data with an RCS value of $\chi^2_\nu = 0.633$ (3sf) giving a saturation power $P_{\text{sat}} = 610 \pm 180$ $\mu$W. Power broadening was clearly observed and shown to agree with the theoretical expression given by Eq. (13) with an RCS value of $\chi^2_\nu = 0.0878$ (3sf) giving a saturation power of $P_{\text{sat}} = 590 \pm 180$ $\mu$W.

The natural linewidth was determined to be $\Gamma = 8.18 \pm 0.51$ MHz which is greater than the theoretical value of $\Gamma = 5.746(8)$ MHz. It has been shown that this discrepancy is not caused by pressure broadening or broadening as a result of the Zeeman effect but rather transit time broadening as well as broadening due to the recoil effect.

The obtained curves showing the variation of peak amplitude $A_0$ and power broadened FWHM $\Gamma$ against the total incident power show the tradeoff between the signal to noise ratio and the linewidth resolution. The curves can be used in optimising the power of the pump beam in future Doppler-free spectroscopy experiments.

The setup can be improved with the use of a balanced photodiode detector instead of detectors PD1 and PD2 which would allow for higher sensitivity and reduce the number of datasets required for a measurement. An alternative frequency calibration can be performed by modulating the laser with a radio frequency (RF) signal which would result in additional peaks either side of the transition and crossover peaks separated by the frequency of the RF signal.

In the future the investigation should be extended to also study the effects of varying the power of the probe beam and both the pump and probe beams. Investigating the effects on the crossover peaks would be particularly interesting since for those the pump and probe beams are each in resonance with a different hyperfine transition.

Finally, the broadening caused by the recoil effect can be eliminated by employing Doppler-free 2-photon spectroscopy in which 2 counter propagating photons are absorbed simultaneously resulting in no change in the linear momentum of the atom [18].

## REFERENCES


[1] A. Akulshin, V. Sautenkov, V. Velichansky, A. Zibrov, and M. Zverkov, "Power broadening of saturation absorption resonance on the d2 line of rubidium," *Optics communications*, vol. 77, no. 4, pp. 295–298, 1990.

[2] J. E. Sansonetti and W. C. Martin, "Handbook of basic atomic spectroscopic data," *Journal of physical and chemical reference data*, vol. 34, no. 4, pp. 1559–2259, 2005.

[3] D. A. Steck, "Rubidium 85 d line data," [Online]. Available: https://steck.us/alkalidata/, 2023.

[4] C. J. Foot, *Atomic Physics*. OUP Oxford, 2004, vol. 7.

[5] T. Rieger and T. Volz, "Doppler-free saturation spectroscopy," 2004.

[6] A. C. Melissinos and J. Napolitano, *Experiments in modern physics*. Gulf Professional Publishing, 2003.

[7] H. Khan, "Fabry-pérot interferometer: construction, calibration and developement," 2015.

[8] C. Hawthorn, K. Weber, and R. E. Scholten, "Littrow configuration tunable external cavity diode laser with fixed direction output beam," *Review of scientific instruments*, vol. 72, no. 12, pp. 4477–4479, 2001.

[9] K. MacAdam, A. Steinbach, and C. Wieman, "A narrow-band tunable diode laser system with grating feedback, and a saturated absorption spectrometer for cs and rb," *American Journal of Physics*, vol. 60, no. 12, pp. 1098–1111, 1992.

[10] L. Kostal, "Doppler-free Spectroscopy of Rubidium GitHub repository," [Online]. Available: https://github.com/KostalLukas/Doppler-free-Spectroscopy-of-Rubidium, 2024.

[11] S.-J. Baek, A. Park, Y.-J. Ahn, and J. Choo, "Baseline correction using asymmetrically reweighted penalized least squares smoothing," *Analyst*, vol. 140, no. 1, pp. 250–257, 2015.

[12] P. T. Boggs, P. T. Boggs, J. E. Rogers, and R. B. Schnabel, "User's reference guide for odrpack version 2.01: Software for weighted orthogonal distance regression," 1992.

[13] D. A. Steck, "Rubidium 87 d line data," [Online]. Available: https://steck.us/alkalidata/, 2003.

[14] M. Shi, T. Wang, Y. Liu, and X. Wang, "Broadening and shifting of rb d1 and d2 line in low pressure vapor cell," *Optik*, vol. 183, pp. 751–756, 2019.

[15] J. Bergquist, *Doppler Free Spectroscopy*. Academic Press , St. Louis, MO, 1996-01-01 1996, no. 29.

[16] A. A. M. P. J. F. R. V Jacques, B Hingant, "Nonlinear spectroscopy of rubidium: an undergraduate experiment," *European journal of physics*, vol. 30, no. 5, p. 921, 2009.

[17] J. Shirley, "Recoil effects on doppler-free lineshapes in non-linear spectroscopy," *Journal of Physics B: Atomic and Molecular Physics*, vol. 13, no. 8, p. 1537, 1980.

[18] J. E. Bjorkholm and P. F. Liao, "Line shape and strength of two-photon absorption in an atomic vapor with a resonant or nearly resonant intermediate state," *Phys. Rev. A*, vol. 14, pp. 751–760, Aug 1976.

[19] G. S. Giri, "Laser spectroscopy of rubidium," 2021.


## CYCLE 2 FEEDBACK

The language of this report is clear. An appropriate amount of details is, in general, provided in the text. The figures have clear axis labels and legends and it is nice to see the data and simulation compared in the same plots. A table with uncertainties would have been nice. In some places the choice of words could be improved to make the sentences more precise. The figure captions are very short and can be used to provide more detailed descriptions of the figures.